CrystEngComm

Structural Diversity of Four Lanthanide Metal-Organic Frameworks based on 2,6-Naphthalenedicarboxylate: Synthesis, Structures and Photoluminescent Properties

Journal:	*CrystEngComm*
Manuscript ID	CE-ART-10-2020-001448.R1
Article Type:	Paper
Date Submitted by the Author:	24-Nov-2020

Complete List of Authors:	Chatenever, Ana; University of California, Santa Cruz, Department of Chemistry and Biochemistry Matsuoka, Joe; University of California, Santa Cruz, Department of Chemistry and Biochemistry Wang, Stanley; University of California, Santa Cruz, Department of Chemistry and Biochemistry Ehlke, Beatriz; University of California, Santa Cruz, Department of Chemistry and Biochemistry LeMagueres, Pierre; Rigaku Americas Corporation Reinheimer, Eric; Rigaku Americas Song, Xuelin; Tongji University, Department of Chemistry Fei, Honghan; Tongji University, Department of Chemistry Oliver, Scott; University of California, Santa Cruz, Department of Chemistry and Biochemistry

Structural Diversity of Four Lanthanide Metal-Organic Frameworks based on 2,6-Naphthalenedicarboxylate: Synthesis, Structures and Photoluminescent Properties

Ana R. K. Chatenever[†], Joe E. Matsuoka[†], Stanley J. Wang[†], Beatriz Ehlke[†], Pierre Le Maguerès[§], Eric W. Reinheimer[§], Xueling Song[⊥], Honghan Fei[⊥] and Scott R. J. Oliver[*†]

† University of California, Santa Cruz, Department of Chemistry and Biochemistry, 1156 High Street, Santa Cruz, California 95064

§ Rigaku Americas Corporation, 9009 New Trails Drive, The Woodlands, Texas 77381

⊥ Tongji University, School of Chemical Science and Engineering, 1239 Siping Road, Shanghai, China 200092

Abstract

We report the crystal structures of four different neutral lanthanide (Ln = La, Nd, Eu and Gd) metal-organic frameworks based on the organic linker 2,6-naphthalenedicarboxylate (NDC). The materials are three-dimensional and crystallize in three distinct topologies, with distinct bonding modes of NDC and lanthanide coordination numbers ranging from seven to nine and varying geometry. We denote our materials **SLUG-49** [$La_6(NDC)_9(DMF)_3 \cdot 6$ DMF], **-50** [$Nd_2(NDC)_3O(DMF)_2$], **-51** [$Eu_2(NDC)_3(DMF)_2 \cdot$DMF], and **-52** [$Gd_4(NDC)_6(DMF)_4$] (DMF = N,N-dimethylformamide). The structures exhibit similar thermal decomposition profiles and

infrared spectra. The Eu(III)-based material exhibits a sharp red-orange luminescence at 613 nm with a quantum efficiency of 3.56%.

Introduction

Metal-organic frameworks (MOFs) are a class of robust, crystalline three-dimensional materials. MOFs are constructed from metal nodes connected by organic linkers which give rise to a porous extended framework. Due to their inherent pore volume, MOFs have potential applications in ion exchange, sensing, gas storage and catalysis.[1–5] Lanthanide-based MOFs have attracted attention in recent years due to their large coordination numbers and luminescent applications, particularly with Eu^{3+} and Tb^{3+}.[6–9] The lanthanide ions Eu^{3+} and Tb^{3+} are excellent phosphors when paired with a conjugated linker due to ligand to metal charge transfer (LMCT).[6,8,10] The excited states of Eu^{3+} and Tb^{3+} exhibit sizeable gaps between the lowest ground state and first excited state, which allow them to emit in the visible red and green wavelength range, respectively.[11] Luminescent MOFs are potential candidates for sensing of analytes that disrupt or shift the emission of the MOF.

Naphthalenedicarboxylate (NDC) has been studied as an organic linker in lanthanide-based MOFs.[12–21] Different solvent systems, temperatures, and ratios of metal to ligand have resulted in dozens of distinct structures. Ln-NDC structures are typically neutral in charge and are coordinated by solvent molecules such as DMF or H_2O. The MOFs $\{[Ln_2(NDC)_3(H_2O)_4]\cdot(DMF)_4$, Ln = Eu, Gd, Tb, Dy, Er, Yb, Lu, Y$\}$ reported by Zhang and coworkers demonstrated that the Eu-based material was capable of sensing organic solvent molecules. The activated Gd-based material (after heating to 200 °C for two hours to remove

uncoordinated DMF) exhibited an adsorption capacity for cationic and anionic organic dyes such as crystal violet, methylene blue, methylene orange, and rhodamine B in water.[21] These frameworks are isomorphous and exhibit eight-coordinate lanthanide(III) centers with rhombic channels along the *b*-axis.

The Tang group reported three structures formed from a sulfonyl-functionalized NDC ligand (4,8-disulfonyl-2,6-naphthalenedicarboxylic acid, H_4-DSNDA).[22] Using eight different lanthanides and similar reaction conditions, three distinct structures were synthesized: $\{[Pr_4(OH)_4(DSNDA)_2(H_2O)_{12}](H_2O)_{10}$, $[Ln(H_2\text{-}DSNDA)_{0.5}(DSNDA)_{0.5}(H_2O)_5]$ (Ln = La, Nd, Sm, Eu, Gd, Dy) and $[Er(H\text{-}DSNDA)(H_2O)_4](H_2O)\}$. The first structure is three-dimensional, while the other two are two-dimensional. The diversity of structures is explained by the several different coordination modes of the H_4-DSNDA ligand, which can coordinate to lanthanides through both the carboxylate and sulfonate groups.

Here, we discuss the structures and properties of four new lanthanide MOFs. The materials differ slightly in their structures but all contain naphthalenedicarboxylate (NDC) as the organic linker and the solvent dimethylformamide (DMF) as a linker and/or coordinated within the pore volume. All materials were characterized by single crystal X-ray diffraction (SCXRD), powder XRD (PXRD), thermogravimetric analysis (TGA) and Fourier transform infrared spectroscopy (FTIR). The luminescence of the Eu-based material was additionally characterized by photoluminescence spectroscopy.

Experimental Section

Reagents. Lanthanum (III) nitrate hexahydrate [$La(NO_3)_3 \cdot 6H_2O$, Alfa Aesar, 99%], neodymium (III) nitrate hexahydrate [$Nd(NO_3)_3 \cdot 6H_2O$, Alfa Aesar, 99.9%], europium (III) nitrate hexahydrate [$Eu(NO_3)_3 \cdot 6H_2O$, Strem Chemicals, 99.9%], gadolinium (III) nitrate hexahydrate [$Gd(NO_3)_3 \cdot 6H_2O$, Strem Chemicals, 99.9%], 2,6-naphthalenedicarboxylic acid [$HO_2C(C_{10}H_6)CO_2H$], TCI America, > 98%] and N,N-dimethylformamide [$(CH_3)_2NCHO$, Macron Fine Chemicals, Analytical Reagent] were used as-received.

Synthesis. [$Ln_2(NDC)_2(DMF)_2 \cdot x$ DMF] (Ln = La, Nd, Eu, Gd, which we denote as SLUG-49, -50, -51 and -52, respectively, for the University of California, Santa Cruz–structure number) were synthesized under solvothermal conditions. A mixture of $Ln(NO_3)_3 \cdot xH_2O$ (0.200 g or equimolar amount of other metal salt), 2,6-NDC (0.197 g) and 10.0 mL DMF was stirred until homogeneous. The mixture was transferred into an autoclave and heated statically under autogenous pressure for 3 d at 110 to 125 °C, then slow cooled to room temperature at a rate of 0.1 °C/min. After vacuum filtering and rinsing with ethanol, lustrous, block-shaped crystals suitable for SCXRD were collected among a powder of smaller crystals of the same phase.

Instrumental. A small colourless plate-like crystal of **SLUG-51** with dimensions 0.014 x 0.047 x 0.062 mm^3 was secured within a thin layer of Paratone oil inside a 20 μm fiber loop micromount. Single crystal X-ray diffraction data was collected at 100 K using micro-focused Mo $K_{\alpha 1}$ radiation (= 0.71073 Å) on a Rigaku XtaLAB Synergy-S X-ray diffractometer equipped with a HyPix-6000HE hybrid photon counting (HPC) detector. A data collection strategy to ensure maximum completeness and adequate redundancy was determined using CrysAlis^{Pro}.[23] 458 images were collected in 4 different scans with an exposure time of 140 sec / 0.5°. Data

processing was performed using CrysAlis^{Pro} as well and included an empirical multi-scan absorption correction applied using the SCALE3 ABSPACK scaling algorithm.[24] The structure was solved *via* intrinsic phasing methods using ShelXT and refined using ShelXL within the Olex2 graphical user interface.[25–27] The final structural refinements were carried out to 0.837 Å and included anisotropic temperature factors on all non-hydrogen atoms. Hydrogen atoms were attached via the riding model at calculated positions using suitable HFIX commands. The other three structures were solved by the same methods.

PXRD patterns were obtained on a Rigaku Miniflex II Plus diffractometer with Cu-Kα radiation (λ = 1.5418 Å) from 2° to 35° or 60° (2θ) at a rate of 2°/min and a step size of 0.02°. TGA was performed on a TA Q500 Thermoanalyzer. Samples were heated in a platinum pan at a ramp rate of 10 °C/min under nitrogen flow. The samples for *ex situ* variable temperature (VT-) PXRD were heated in a tube furnace to the designated temperature at a rate of approximately 2 °C/min in air. FTIR spectroscopy of the materials was collected on a PerkinElmer spectrophotometer using KBr pellets. Steady-state photoluminescence spectra were obtained at room temperature on an Edinburgh Instruments FLS980 spectrophotometer. Absolute PLQE measurements of both bulk and microscopic crystals were performed on a FLS920 spectrophotometer with an integrating sphere ($BaSO_4$ coating) using single photon counting mode. The focal length of the monochromator was 300 mm. SLUG-51 (Eu) was excited at 360 nm using a 450W Xenon lamp with 3 mm excitation slit width and detected by a Hamamatsu R928p photomultiplier tube. The emission was obtained using 0.2 nm scan step, 0.2 s scan dwell time, and 0.1 mm emission slit width. The PLQEs were calculated by equation 1:

$$\varphi = k_f / k_a \qquad [1]$$

where kf is the number of emitted photons and ka is the number of absorbed photons. CHN elemental analysis: SLUG-49 (La): calculated (%): C 47.01, H 3.37, N 3.66; observed (%): C 46.62, H 3.47, N 3.49. SLUG-50 (Nd): calculated (%): C 46.14, H 2.96, N 2.56; observed (%): C 46.18, H 3.52, N 3.30. SLUG-51 (Eu): calculated (%): C 46.36, H 3.38, N 3.61; observed (%): C 45.86, H 3.03, N 2.69. SLUG-52 (Gd): calculated (%) C 45.72, H 2.93, N 2.54; observed (%) C 56.55, H 2.76, N <0.05.

Results and Discussion

Synthesis. SLUG-49 through 52 were synthesized solvothermally in good yields (75% to 84% based on Ln^{3+}) at a synthesis temperature of 110 to 125 °C. Below this optimal range, no crystalline product formed, while in the case of SLUG-52 (Gd) an additional crystalline phase formed but not of sufficient size for SCXRD (*vide infra*). All crystals were colorless blocks among a powder of the same phase (Figure S1). Quenching instead of slow cooling gave rise to no product.

Structure. Single crystal structures of the MOFs based on La, Nd, Eu and Gd (SLUG-49 through 52) were solved (Figures 1-4) and the crystal data for these structures are summarized in Table 1. All four are neutral in charge and each crystallizes in a distinct space group and structure. Throughout all four structures, two distinct binding modes of the NDC ligand are observed, which we refer to as type I and type II coordination (Figure 5). The SCXRD data reveals the La-based structure (SLUG-49) crystallizes in the $P\bar{1}$ space group. There are three distinct La^{3+} ions in the asymmetric unit of SLUG-49, each of which is coordinated to eight oxygens with a distorted square antiprismatic geometry. La(1) is coordinated by four oxygens

from NDC ligands *via* type I coordination, two bridging NDCs with type II coordination, an oxygen from a DMF molecule, and a disordered oxygen that μ-2 connects to La(3). La(2) is coordinated by six oxygens from NDC *via* type I coordination, one oxygen from a DMF molecule, and one terminal oxygen. La(3) is coordinated to four NDC ligands *via* type I coordination, one type II NDC, two DMF molecules and the disordered oxygen that μ-2 connects to La(1). SLUG-49 contains 6 disordered floating DMF molecules per formula unit.

The Nd- and Eu-based structures (SLUG-50 and -51, respectively) are the most similar to each other. Both are in the monoclinic crystal system but the structures crystallize in the *C*2/*c* and $P2_1/n$ space groups, respectively. SLUG-50 contains only one type of nine-coordinate monocapped square antiprismatic Nd^{3+} center, surrounded by four NDC ligands with type I coordination, two type II NDCs, one DMF molecule and one oxygen that μ-2 bridges to a neighbouring Nd^{3+}. The latter inorganic connectivity is not extended and gives rise to dimers. SLUG-51 is characterized by eight-coordinate Eu^{3+} centers. Here, two crystallographically unique distorted square antiprismatic Eu^{3+} centers are surrounded by five type I NDCs, two type II NDC and one DMF molecule. Unlike SLUG-50, SLUG-51 also contains a floating DMF molecule. Lastly, the Gd-based SLUG-52 structure crystallizes in the orthorhombic $Pca2_1$ space group. All four crystallographically unique Gd^{3+} centers are seven-coordinate distorted pentagonal bipyramidal [although Gd(2) and Gd(4) are better described as distorted monocapped trigonal prismatic], surrounded by six NDC ligands with type I coordination and one DMF molecule. Syntheses with cerium and erbium were also attempted but no crystals large enough for SCXRD could be isolated.

Table 1. Crystal Data and Structure Refinement for SLUG-49, -50, -51 and -52

Material	SLUG-49	SLUG-50	SLUG-51	SLUG-52
Empirical Formula	$La_6C_{135}H_{121}O_{47}N_9$	$NdC_{21}H_{16}O_{7.5}N$	$Eu_2C_{45}H_{39}O_{15}N_3$	$Gd_4C_{84}H_{64}O_{28}N_4$
Formula Weight ($g \cdot mol^{-1}$)	3454.86	546.59	1165.71	2206.39
Temperature (K)	100(2)	100(2)	100.01(10)	120(2)
Crystal System	Triclinic	Monoclinic	Monoclinic	Orthorhombic
Space Group	$P\bar{1}$	$C2/c$	$P2_1/n$	$Pca2_1$
a, b, c, (Å)	13.2526(8) 14.3785(8) 19.9214(10)	12.4204(5) 21.5953(7) 16.3081(6)	11.9185(3) 21.8730(5) 16.5342(4)	19.4366(9) 8.7643(4) 45.084(2)
α, β, γ (°)	70.927(5) 74.630(5) 75.542(5)	90 102.907(4) 90	90 100.476(2) 90	90 90 90
Volume ($Å^3$)	3403.5(4)	4263.7(3)	4238.51(18)	7679.9(6)
Z	1	8	4	4
ρ_{calc} ($g \cdot cm^{-3}$)	1.686	1.703	1.827	1.908
μ (mm^{-1})	14.980	2.480	3.009	3.500
F(000)	1712	2152	2304	4304
Crystal Dimensions (mm)	0.029 × 0.043 × 0.052	0.065 × 0.077 × 0.092	0.014 × 0.047 × 0.062	0.037 × 0.058 × 0.095
Index Ranges	$-12 \le h \le 15$ $-16 \le k \le 17$ $-23 \le l \le 23$	$-16 \le h \le 16$ $-27 \le k \le 29$ $-22 \le l \le 21$	$-14 \le h \le 14$ $-26 \le k \le 27$ $-20 \le l \le 20$	$-25 \le h \le 24$ $-11 \le k \le 11$ $-59 \le l \le 60$
Reflections Collected	11945	4360	30302	19055
Unique Data	9215 [R_{int} = 0.0589]	3954 [R_{int} = 0.0296]	6543 [R_{int} = 0.0249]	13636 [R_{int} = 0.0918]
Data/Restraints/Parameters	11945 / 111 / 1108	4360 / 38 / 316	8660 / 0 / 592	19055 / 1119 / 1128
Goodness of Fit on F^2	1.047	1.075	1.025	1.005
Final R Factors [I > 2σ(I)]	R_1 = 0.0430 wR_2 = 0.1030	R_1 = 0.0254 wR_2 = 0.0675	R_1 = 0.0220 wR_2 = 0.0462	R_1 = 0.0508 wR_2 = 0.0842
Largest Residual Peak/Hole ($e \cdot Å^{-3}$)	1.128 / -1.187	1.043 / -0.640	0.639 / -0.720	2.085 / -1.329

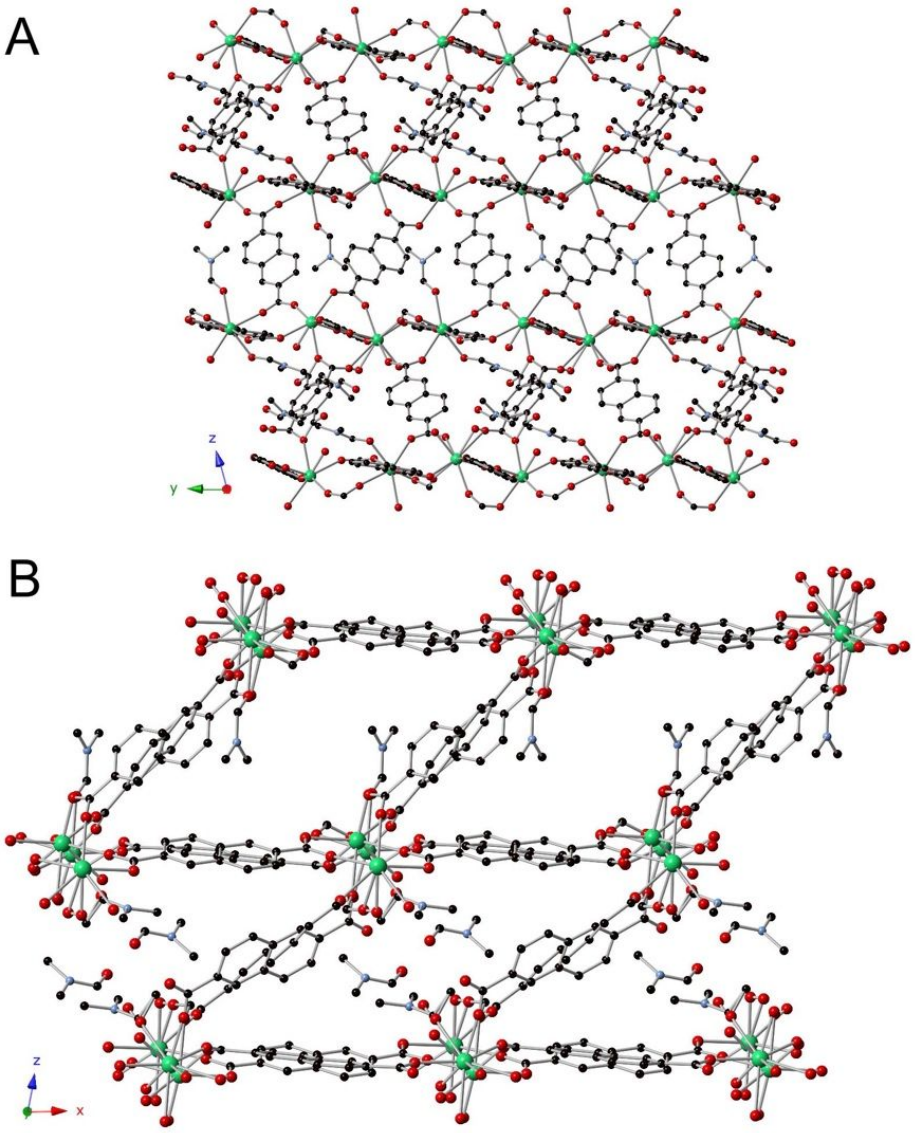

Figure 1. Crystallographic projections of SLUG-49 (La): A) View along the *a*-axis, highlighting the binding modes of NDC and the three-dimensionally extended connectivity; B) View along the *b*-axis, showing the three crystallographically distinct La centers and floating DMF molecules within the pores (La – green; O – red; C – black; N – light blue; H – omitted for clarity).

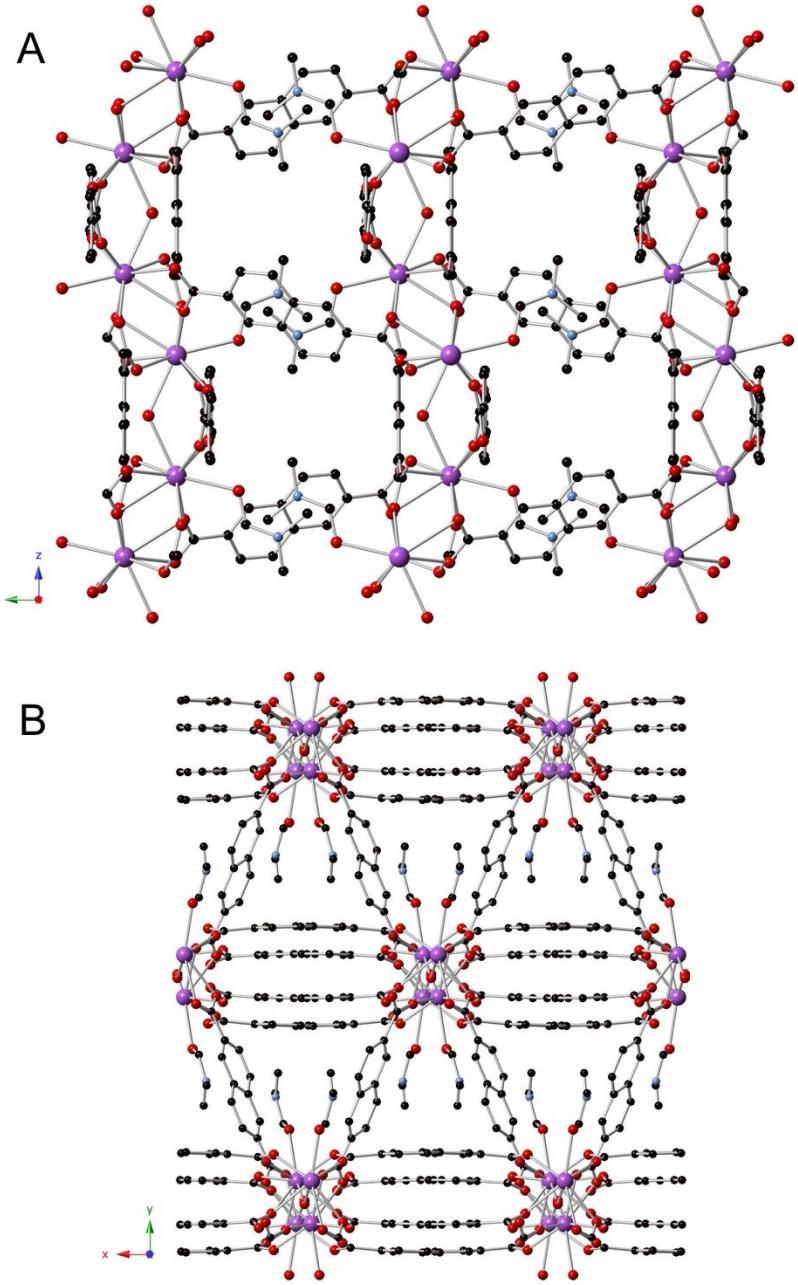

Figure 2. Crystallographic projection of SLUG-50 (Nd): A) View along the *a*-axis of the three-dimensional structure; B) View along the *c*-axis, highlighting the various binding modes and π-stacking of NDC ligands, as well as the bound DMF molecules (Nd – purple; O – red; C – black; N – light blue; H – omitted for clarity).

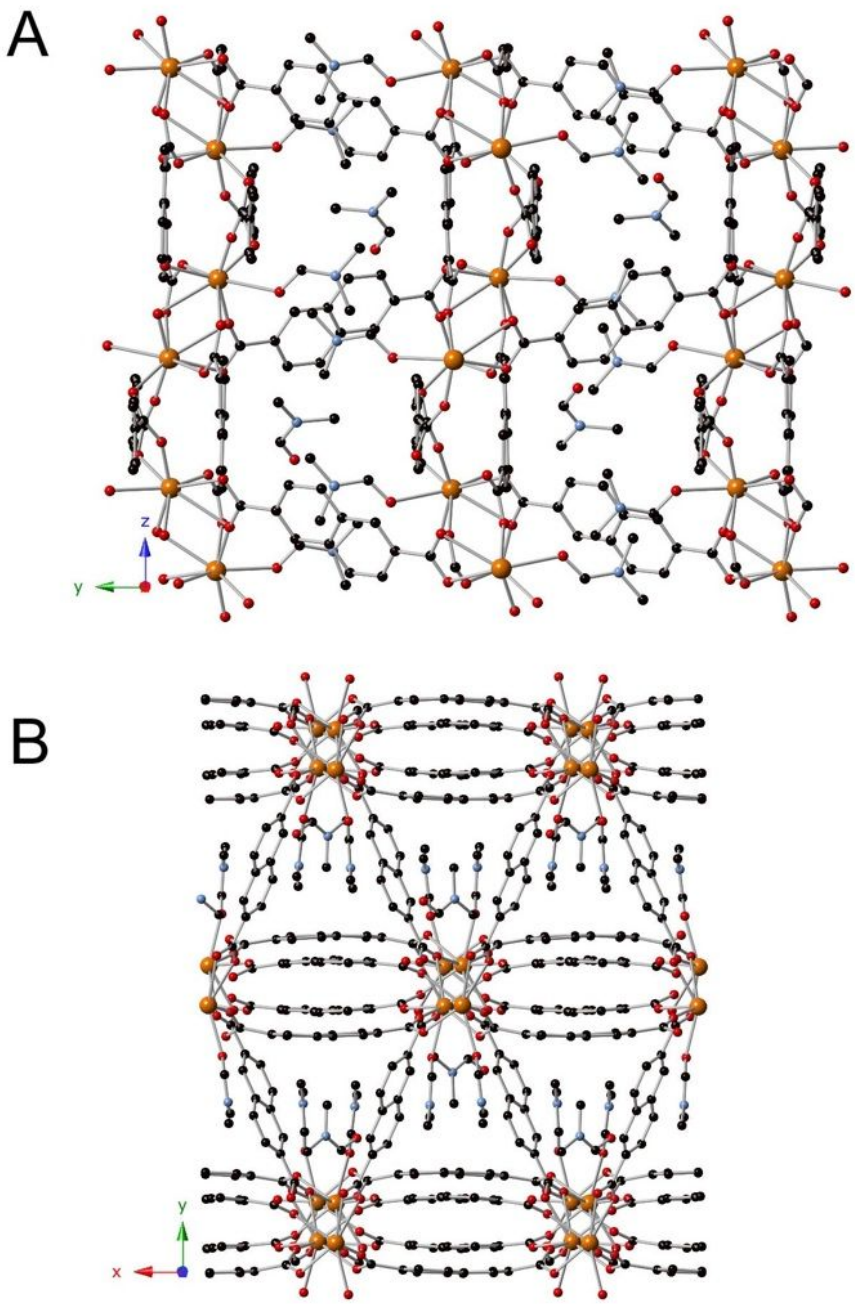

Figure 3. Crystallographic projections of SLUG-51 (Eu): A) View along the *a*-axis of the three-dimensional structure; B) View along the *c*-axis, highlighting the various binding modes and π-stacking of NDC ligands, as well as the bound and floating DMF molecules (Eu – orange; O – red; C – black; N – light blue; H – omitted for clarity).

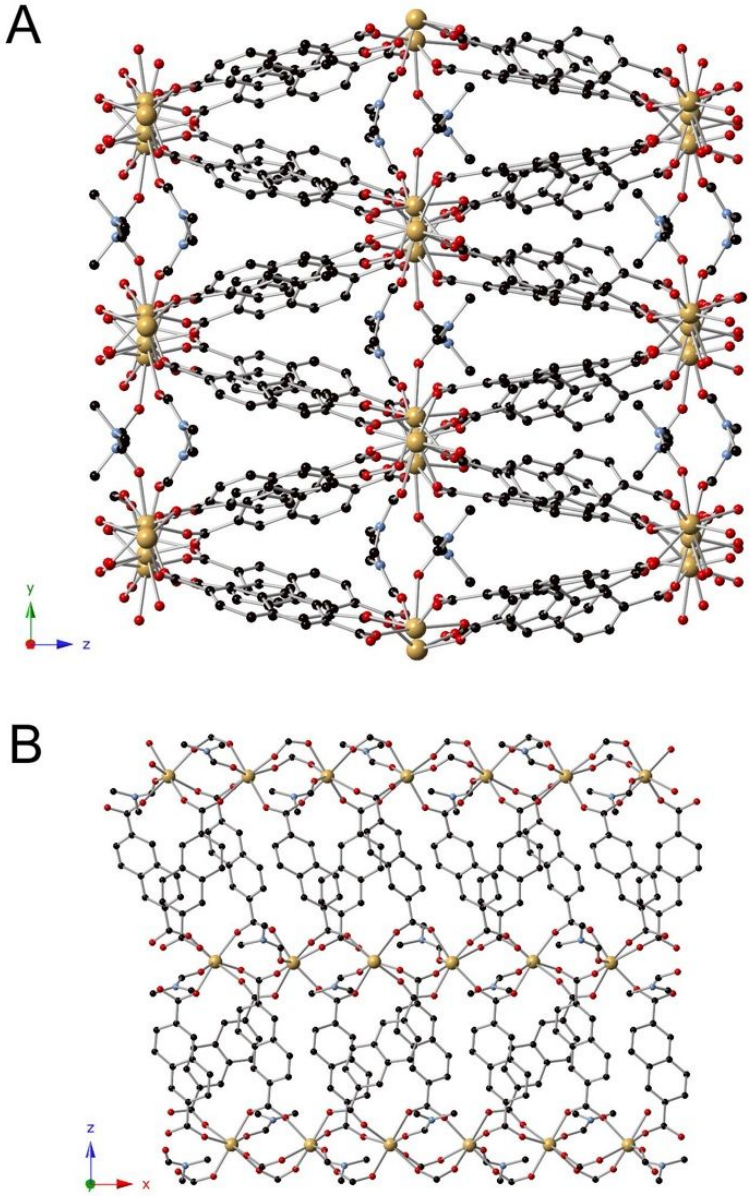

Figure 4. Crystallographic projections of SLUG-52 (Gd); A) View along the *a*-axis of the three-dimensional structure; B) View along the *b*-axis, showing the various binding modes of the NDC ligands and the bound DMF molecules (Gd – yellow; O – red; C – black; N – light blue; H – omitted for clarity).

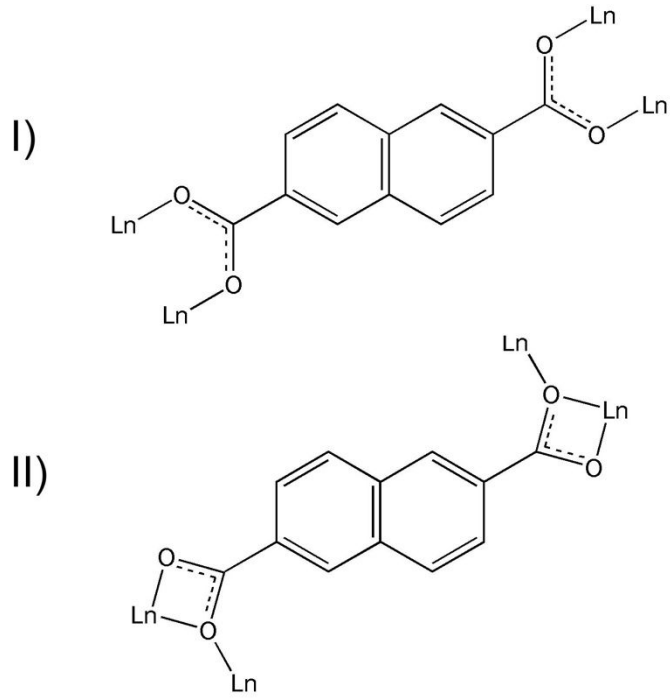

Figure 5. The two binding modes of the NDC ligand in SLUG-49 through 52: I) NDC bridges four lanthanide metal ions where each oxygen is monodentate; II) each carboylate end of the NDC connects to two Ln centers, one in a monodentate manner and the other in a bidentate manner.

PXRD. As evidenced by the SCXRD data, this group of structures is not isomorphous. The PXRD patterns of SLUG-49 through 52 are shown in Figure 6. Comparisons of the theoretical PXRDs with the as-synthesized materials are presented in Figures S2-S5. The as-synthesized PXRD patterns match agreeably with the theoretical PXRD patterns. In Figure S5, however, it is apparent that another phase is present in the as-synthesized SLUG-52 (Gd) as indicated by the peaks near 8.5° and 17° (2θ). Attempts at isolating the other phase for structure solution were unsuccessful.

One possible reason behind the diversity of these structures is due to the rigidity of the NDC ligand. As NDC molecules coordinate to the Ln(III) centers, effects such as π-stacking and an abundance of coordinating DMF solvent molecules compete to fill the coordination sphere of the metal.[28] These competing effects may explain the variation in coordination number and binding modes of the lanthanides observed in these structures. Two of the structures, SLUG-50 (Nd) and SLUG-51 (Eu) exhibit π-stacking among the NDC ligands (Figures 2B, 3B). Half of the NDC rings exhibit π-stacking at a distance of ~ 3.7 Å (Figure S6). These intermolecular forces likely play a role in establishing the long-range order among these structures and stabilize the various lanthanide coordination spheres. As the NDC ligands and DMF molecules compete for coordination with the lanthanides, the π-stacking of the NDC ligands likely further stabilizes these structures.

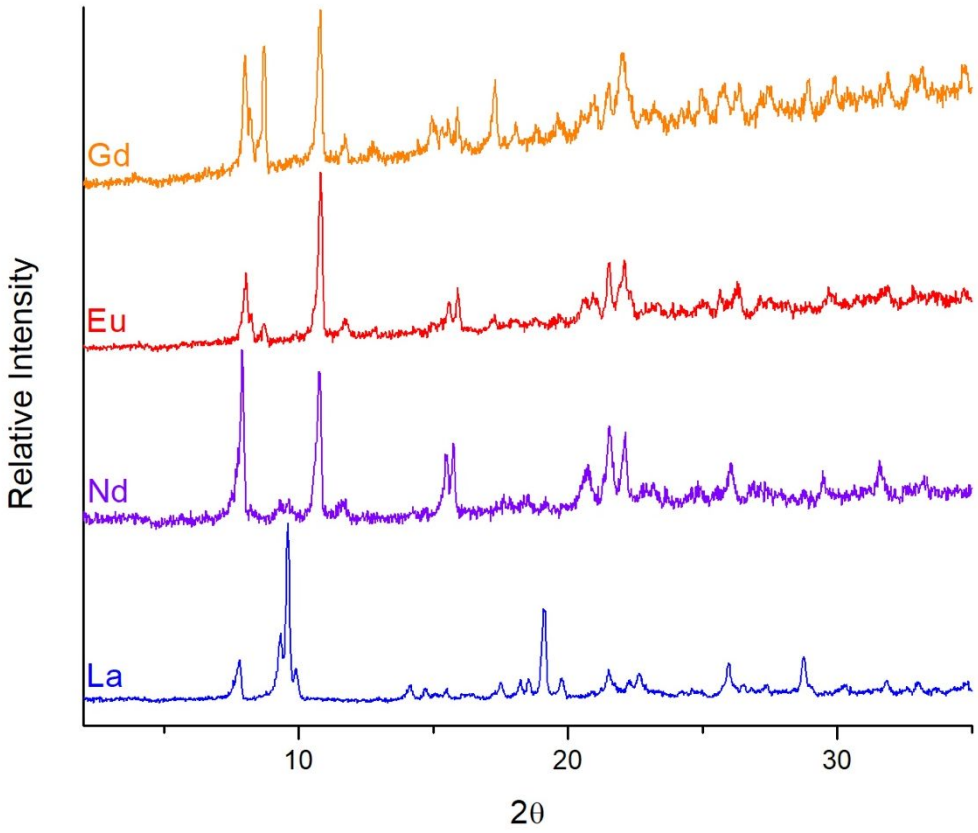

Figure 6. PXRD patterns of SLUG-49 through 52.

Thermal characterization. The four materials exhibit similar decomposition profiles, which can be characterized by the loss of free occluded DMF, followed by the loss of coordinated DMF molecules and finally the loss of the organic NDC linker (Figure 7). In the case of SLUG-49 (La), a 12.7% mass loss by 210 °C is observed (Figure 7A). This corresponds well with the loss of the six free DMF solvent molecules, which represents a theoretical mass loss of 12.7%. An additional 7.8% mass is lost by 290 °C, which corresponds the three coordinated DMF molecules (theoretical mass loss: 7.3%), with an unknown intermediate in the VT-PXRD at 300 °C (Figure 7B). Lastly, there is a loss of 51.4% mass by 600 °C, which can be attributed to the loss of the

organic NDC linkers (theoretical: 52.6%). VT-PXRD shows that the final phase is La_2O_3 (ICDD PDF #022-0367) (Figure 7B, top pattern at 600 °C).

In the case of SLUG-50 (Nd), a mass loss of 3.0% is observed at 180 °C due to the evolution of free DMF molecules. At 290 °C, an additional 13.1% mass loss is observed which corresponds to the loss of coordinated DMF molecules (theoretical:13.4%). By 600 °C, the observed mass loss of 39.7% corresponds to the theoretical mass loss of 41% of the organic component. SLUG-51 (Eu) loses 5.5% by 180 °C, which is attributed to the free DMF molecule (theoretical: 6.2%. At 310 °C, a mass loss of 12.4% is observed, which matches nicely with the theoretical loss of 12.5% and corresponds to the loss of the two coordinated DMF molecules. By 600 °C, a mass loss of 29.5% is observed. This last loss corresponds to the organic component, with a theoretical mass loss of 38%. It is evident from the TGA and VT-PXRD (Figure 7E,F) that not all of the organic component has been completely decomposed by 600 °C. SLUG-52 (Gd) loses 6.1% by 175 °C, corresponding to the mass loss of two free DMF molecules (theoretical: 6.6%). The second mass loss is 10.3%, which is attributed to the loss of the three coordinated DMF molecules (theoretical: 9.9%). In the final decomposition step, a mass loss of 37.7% is observed by 600 °C. This corresponds to the partial loss of the organic component, which again is not completely decomposed (Figure 7G,H). In terms of chemical stability, all materials displayed similar behaviour in water, boiling water, acidic aqueous (pH 4.6) and basic aqueous (pH 9.6) under static conditions for 2 h. The PXRD peaks were significantly shifted and broadened, likely due to loss of occluded DMF solvent molecules (Figure S7).

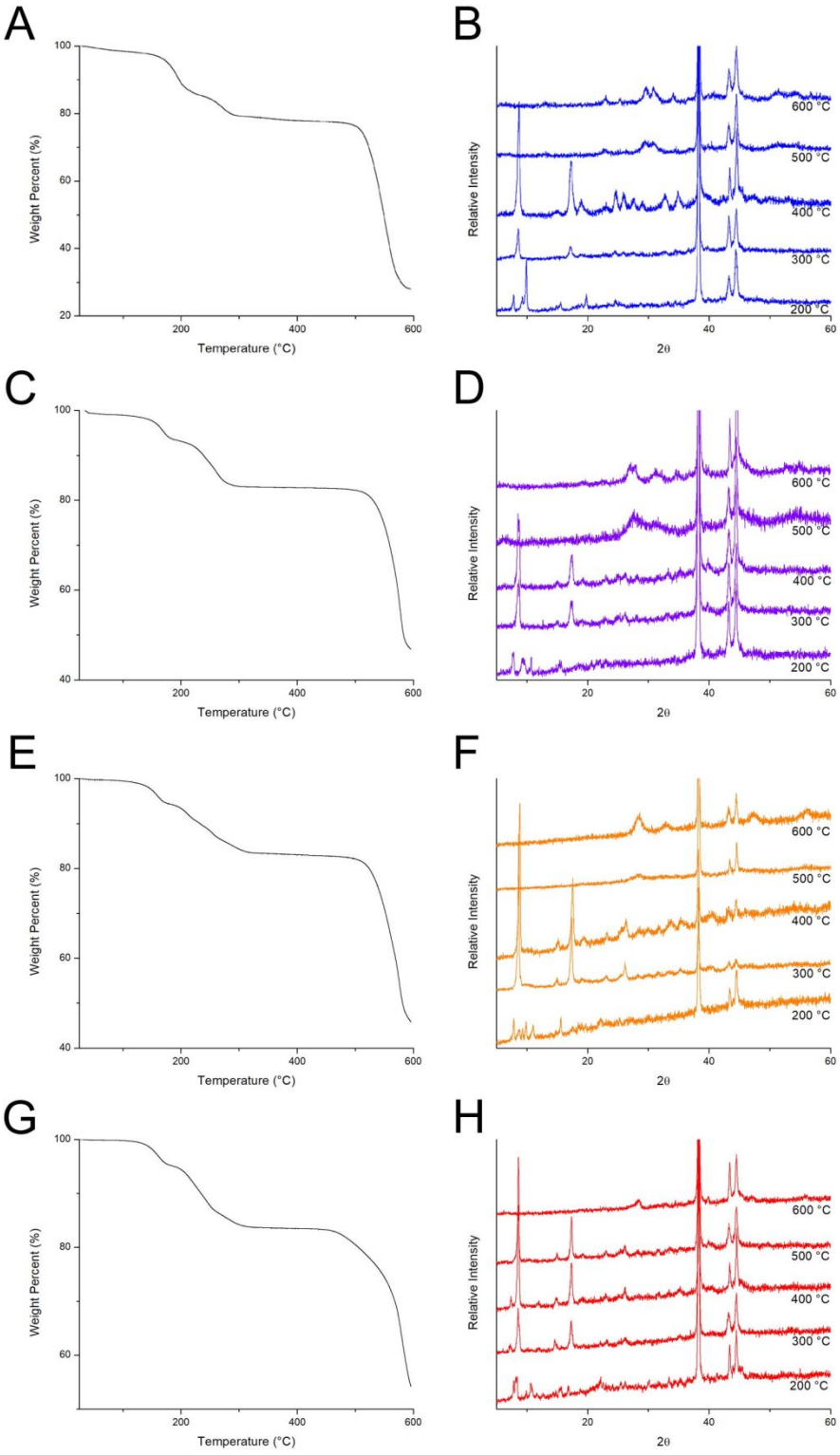

Figure 7. TGA traces and VT-PXRD of SLUG-49 through 52. A-B) SLUG-49 (La); C-D) SLUG-50 (Nd); E-F) SLUG-51 (Eu); G-H) SLUG-52 (Gd).

Vibrational Spectroscopy. Although SLUG-49 through 52 display different structures, their IR spectra are very similar since they all contain NDC ligands and bound/free DMF molecules. Between the range of 1620 to 1680 cm^{-1}, two bands are observed which correspond to the C=O stretch of DMF.[29] The peaks at ~ 1600 cm^{-1} correspond to asymmetrical $(C{-\!-}O)_2$ stretching from the carboxylate group on NDC. The sharp peaks near 1400 cm^{-1} are attributed to the C-N stretch of DMF. The bands between 770 and 790 cm^{-1} correspond to C-H bands on the β-substituted naphthalenes (Figure 8, *cf.* Figure S8).

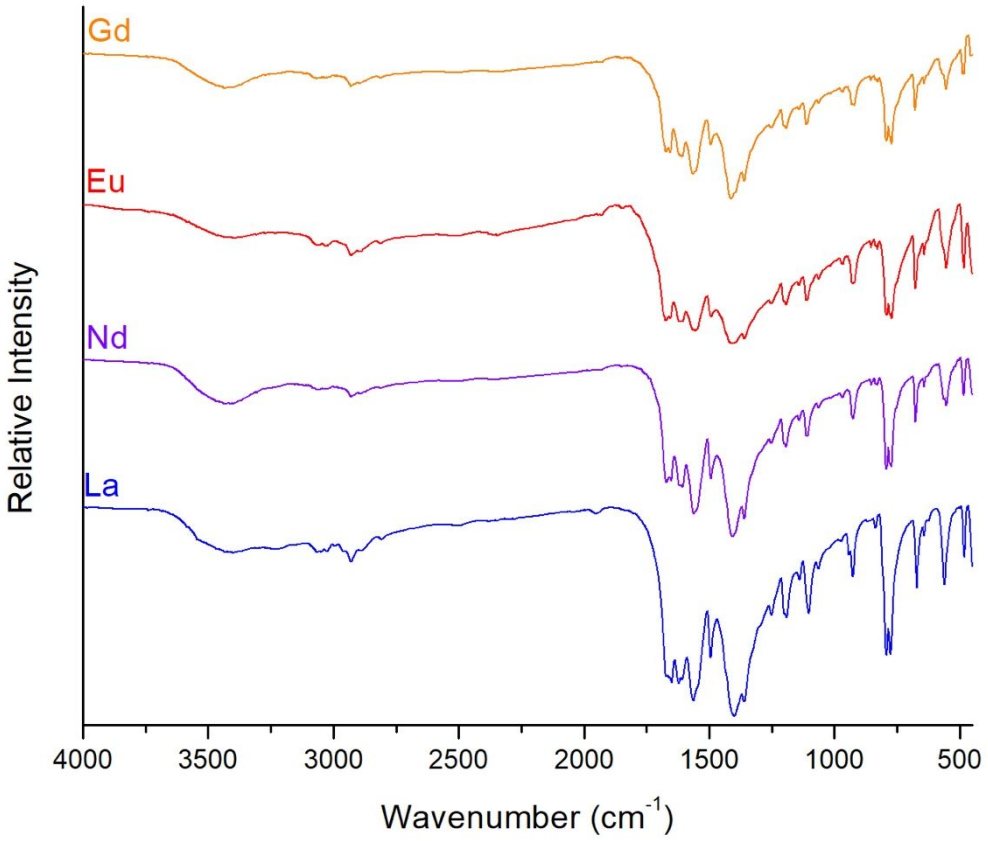

Figure 8. FTIR spectra of SLUG-49 (bottom) through -52 (top).

Photoluminescence. The Eu(III)-based MOF, SLUG-51, exhibits intense luminescence in the visible red-orange region (Figure 9). These emission bands are due to $^5D_0 \rightarrow {}^7F_J$ (J = 1, 2, 4) electronic transitions. The $^5D_0 \rightarrow {}^7F_3$ transition is weakly observed at 660 nm. These electronic transitions are known to be the most notable for Eu(III) complexes.[30] SLUG-51 displays a quantum efficiency of 3.56%. This fluorescence is due to a ligand to metal charge transfer process that is well-known for europium-based compounds. As expected, none of the SLUG-49 (La), SLUG-50 (Nd), or SLUG-52 (Gd) materials were fluorescent. We conducted physisorption analysis of SLUG-51 but the trace showed no uptake (Figure S9) despite the significant void volumes calculated by PLATON (Table S1).

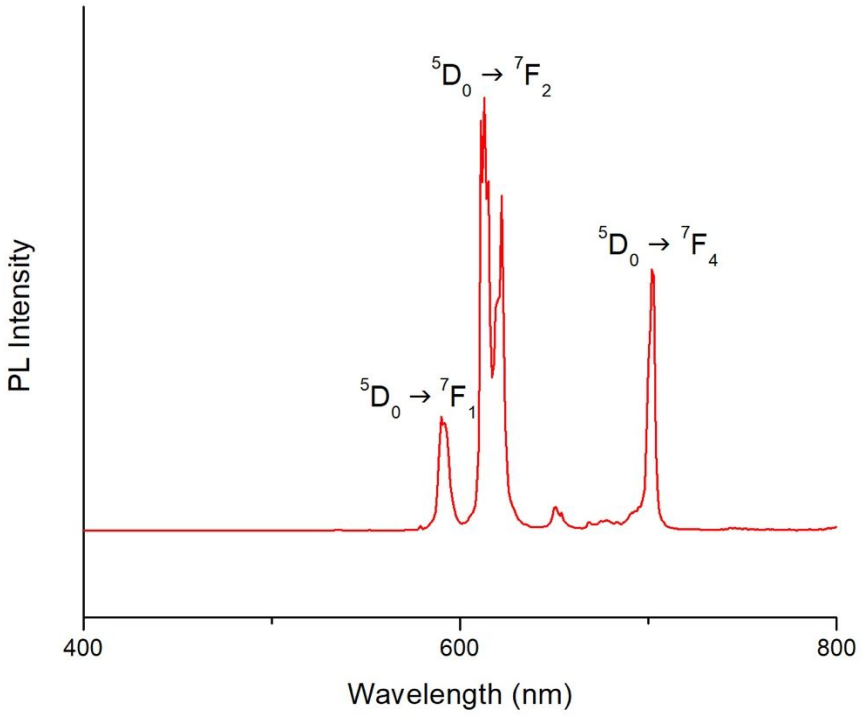

Figure 9. Solid state fluorescence emission spectrum of SLUG-51 (Eu), excited at 362 nm.

Conclusions

We presented four new MOF structures based on lanthanides and the organic linker 2,6-naphthalenedicarboxylate. Each structure is neutral in charge and contains multiple binding modes of NDC and DMF solvent molecules. This work furthers the known chemistry of luminescent metal-organic frameworks that are based on f-block metals. The fact that four different structures were formed indicates that other motifs and structure types likely await discovery.

Acknowledgements

This work was supported by the National Science Foundation under Grant No. 1603754 from the CBET Environmental Engineering GOALI Program. Images were generated using CrystalMaker® 9 (CrystalMaker Software Ltd., Oxford, England, www.crystalmaker.com).

The CIFs have been submitted to CCDC, Deposition Numbers 2034395 through 2034398.

References

(1) Kumar, P.; Pournara, A.; Kim, K.-H.; Bansal, V.; Rapti, S.; Manos, M. J. Metal-Organic Frameworks: Challenges and Opportunities for Ion-Exchange/Sorption Applications. *Prog. Mater. Sci.* **2017**, *86*, 25–74. https://doi.org/10.1016/j.pmatsci.2017.01.002.

(2) Howarth, A. J.; Liu, Y.; Hupp, J. T.; Farha, O. K. Metal–Organic Frameworks for Applications in Remediation of Oxyanion/Cation-Contaminated Water. *CrystEngComm* **2015**, *17* (38), 7245–7253. https://doi.org/10.1039/C5CE01428J.

(3) Furukawa, H.; Cordova, K. E.; O'Keeffe, M.; Yaghi, O. M. The Chemistry and Applications of Metal-Organic Frameworks. *Science* **2013**, *341* (6149), 1230444. https://doi.org/10.1126/science.1230444.

(4) Kumar, P.; Deep, A.; Kim, K.-H. Metal Organic Frameworks for Sensing Applications. *TrAC Trends Anal. Chem.* **2015**, *73*, 39–53. https://doi.org/10.1016/j.trac.2015.04.009.

(5) Vitillo, J. G.; Atzori, C.; Civalleri, B.; Barbero, N.; Barolo, C.; Bonino, F. Design and Characterization of MOFs (Metal–Organic Frameworks) for Innovative Applications. *Hybrid Organic-Inorganic Interfaces* **2018**. https://doi.org/10.1002/9783527807130.ch10.

(6) D. Allendorf, M.; A. Bauer, C.; K. Bhakta, R.; T. Houk, R. J. Luminescent Metal–Organic Frameworks. *Chem. Soc. Rev.* **2009**, *38* (5), 1330–1352. https://doi.org/10.1039/B802352M.
(7) Rocha, J.; D. Carlos, L.; Almeida Paz, F. A.; Ananias, D. Luminescent Multifunctional Lanthanides-Based Metal–Organic Frameworks. *Chem. Soc. Rev.* **2011**, *40* (2), 926–940. https://doi.org/10.1039/C0CS00130A.
(8) Cui, Y.; Chen, B.; Qian, G. Lanthanide Metal-Organic Frameworks for Luminescent Sensing and Light-Emitting Applications. *Coord. Chem. Rev.* **2014**, *273* (Supplement C), 76–86. https://doi.org/10.1016/j.ccr.2013.10.023.
(9) Pagis, C.; Ferbinteanu, M.; Rothenberg, G.; Tanase, S. Lanthanide-Based Metal Organic Frameworks: Synthetic Strategies and Catalytic Applications. *ACS Catal.* **2016**, *6* (9), 6063–6072. https://doi.org/10.1021/acscatal.6b01935.
(10) Cui, Y.; Yue, Y.; Qian, G.; Chen, B. Luminescent Functional Metal–Organic Frameworks. *Chem. Rev.* **2012**, *112* (2). https://doi.org/10.1021/cr200101d.
(11) Bünzli, J.-C. G.; Piguet, C. Taking Advantage of Luminescent Lanthanide Ions. *Chem. Soc. Rev.* **2005**, *34* (12), 1048–1077. https://doi.org/10.1039/B406082M.
(12) Gangu, K. K.; Maddila, S.; Jonnalagadda, S. B. A Review on Synthesis, Crystal Structure and Functionality of Naphthalenedicarboxylate Ligated Metal-Organic Frameworks. *Inorganica Chim. Acta* **2017**, *466* (Supplement C), 308–323. https://doi.org/10.1016/j.ica.2017.06.038.
(13) Wang, Z.; Jin, C.-M.; Shao, T.; Li, Y.-Z.; Zhang, K.-L.; Zhang, H.-T.; You, X.-Z. Syntheses, Structures, and Luminescence Properties of a New Family of Three-Dimensional Open-Framework Lanthanide Coordination Polymers. *Inorg. Chem. Commun.* **2002**, *5* (9), 642–648. https://doi.org/10.1016/S1387-7003(02)00515-4.
(14) Deluzet, A.; Maudez, W.; Daiguebonne, C.; Guillou, O. Interplane Distances Modulation in Lanthanide-Based Coordination Polymers. *Cryst. Growth Des.* **2003**, *3* (4), 475–479. https://doi.org/10.1021/cg020052v.
(15) Zheng, X.; Sun, C.; Lu, S.; Liao, F.; Gao, S.; Jin, L. New Porous Lanthanide-Organic Frameworks: Synthesis, Characterization, and Properties of Lanthanide 2,6-Naphthalenedicarboxylates. *Eur. J. Inorg. Chem.* **2004**, *2004* (16), 3262–3268. https://doi.org/10.1002/ejic.200400176.
(16) Yang, J.; Yue, Q.; Li, G.-D.; Cao, J.-J.; Li, G.-H.; Chen, J.-S. Structures, Photoluminescence, Up-Conversion, and Magnetism of 2D and 3D Rare-Earth Coordination Polymers with Multicarboxylate Linkages. *Inorg. Chem.* **2006**, *45* (7), 2857–2865. https://doi.org/10.1021/ic051557o.
(17) Łyszczek, R.; Rzączyńska, Z.; Kula, A.; Gładysz-Płaska, A. Thermal and Luminescence Characterization of Lanthanide 2,6-Naphthalenedicarboxylates Series. *J. Anal. Appl. Pyrolysis* **2011**, *92* (2), 347–354. https://doi.org/10.1016/j.jaap.2011.07.006.
(18) Łyszczek, R.; Lipke, A. Microwave-Assisted Synthesis of Lanthanide 2,6-Naphthalenedicarboxylates: Thermal, Luminescent and Sorption Characterization. *Microporous Mesoporous Mater.* **2013**, *168*, 81–91. https://doi.org/10.1016/j.micromeso.2012.09.016.
(19) Liu, Y.-H.; Chien, P.-H. A Series of Lanthanide–Organic Frameworks Possessing Arrays of 2D Intersecting Channels within a 3D Pillar-Supported Packed Double-Decker Network and Co 2+ -Induced Luminescence Modulation. *CrystEngComm* **2014**, *16* (37), 8852–8862. https://doi.org/10.1039/C4CE00461B.

(20) Zhang, Q.; Lei, M.; Yan, H.; Wang, J.; Shi, Y. A Water-Stable 3D Luminescent Metal−Organic Framework Based on Heterometallic [EuIII6ZnII] Clusters Showing Highly Sensitive, Selective, and Reversible Detection of Ronidazole. *Inorg. Chem.* **2017**, *56* (14), 7610–7614. https://doi.org/10.1021/acs.inorgchem.7b01156.
(21) Zhu, Y.; Wang, L.; Chen, X.; Wang, P.; Fan, Y.; Zhang, P. 3D Lanthanide Metal-Organic Frameworks Constructed from 2,6-Naphthalenedicarboxylate Ligand: Synthesis, Structure, Luminescence and Dye Adsorption. *J. Solid State Chem.* **2017**, *251*, 248–254. https://doi.org/10.1016/j.jssc.2017.04.026.
(22) Liu, Q.-Y.; Wang, W.-F.; Wang, Y.-L.; Shan, Z.-M.; Wang, M.-S.; Tang, J. Diversity of Lanthanide(III)–Organic Extended Frameworks with a 4,8-Disulfonyl-2,6-Naphthalenedicarboxylic Acid Ligand: Syntheses, Structures, and Magnetic and Luminescent Properties. *Inorg. Chem.* **2012**, *51* (4), 2381–2392. https://doi.org/10.1021/ic2023727.
(23) *CrysAlisPro*; Rigaku Oxford Diffraction; 2018.
(24) *SCALE3 ABSPACK*; Rigaku Oxford Diffraction; 2017.
(25) Sheldrick, G. M. *Acta Cryst.* **2015**, *A71*, 3.
(26) Sheldrick, G. M. *Acta Cryst.* **2015**, *C71*, 3.
(27) Dolomanov, O. V.; Bourhis, L. J.; Gildea, R. J.; Howard, J. a. K.; Puschmann, H. OLEX2: A Complete Structure Solution, Refinement and Analysis Program. *J. Appl. Crystallogr.* **2009**, *42* (2), 339–341. https://doi.org/10.1107/S0021889808042726.
(28) Díaz-Torres, R.; Alvarez, S. Coordinating Ability of Anions and Solvents towards Transition Metals and Lanthanides. *Dalton Trans.* **2011**, *40* (40), 10742–10750. https://doi.org/10.1039/C1DT11000D.
(29) Silverstein, R. M.; Webster, F. X.; Kiemle, D. J. *Spectrometric Identification of Organic Compounds*, 7th ed.; John Wiley & Sons, Inc., 2005.
(30) Binnemans, K. Interpretation of Europium(III) Spectra. *Coord. Chem. Rev.* **2015**, *295*, 1–45. https://doi.org/10.1016/j.ccr.2015.02.015.

TOC Entry

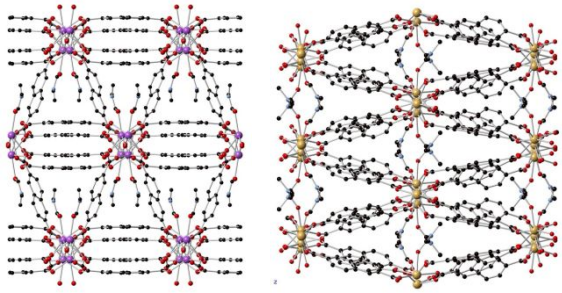

We report four lanthanide metal-organic frameworks based on 2,6-naphthalenedicarboxylate which displays multiple bonding modes, implying more structures await discovery.